Full title: High-throughput profiling identifies resource use efficient and abiotic stress tolerant sorghum varieties

Short title: High-throughput phenotyping reveals abiotic stress responses in sorghum

Kira M. Veley[1], Jeffrey C. Berry[1], Sarah J. Fentress[1], Daniel P. Schachtman[2], Ivan Baxter[1], Rebecca Bart[1]*

[1]Donald Danforth Plant Science Center, Saint Louis, MO 63132

[2]Department of Agronomy and Horticulture and Center for Plant Science Innovation, University of Nebraska–Lincoln, Lincoln, NE 68588

*Corresponding Author (rbart@danforthcenter.org)

ABSTRACT

Energy sorghum (*Sorghum bicolor* (L.) Moench) is a rapidly growing, high-biomass, annual crop prized for abiotic stress tolerance. Measuring genotype-by-environment (G x E) interactions remains a progress bottleneck. High throughput phenotyping within controlled environments has been proposed as a potential solution. Early, measureable indicators of desirable traits that translate to the field would increase the speed of crop improvement efforts. Here we identify shape, color and ionomic indicators of abiotic stress for genetically diverse sorghum varieties. We subjected a panel of 30 sorghum genotypes to either nitrogen deprivation or drought stress and measured responses within an automated phenotyping facility, followed by ionomic profiling. Images of growing plants were collected every day for three weeks, and key metrics are reported. Responses to stress were quantified using differences in shape (16 measureable outputs), color (hue and intensity) and ionome (18 elements). We found shape characteristics to be reliable indicators of performance under both stress conditions tested. In contrast, color was a defining indicator of nitrogen starvation but not drought stress. Through this analysis we were able to measure the speed at which specific genotypes respond to stress and identify individual genotypes that perform most favorably under these stress conditions. These data are made available through an open access, user-friendly, web-based interface. Ionomic profiling was conducted as an independent, low cost and high throughput option for characterizing G x E. The effect of genotype on the ionome was consistent between the two experiments confirming the robustness of the high throughput platform. In addition, multiple individual elements were identified as quantitative outputs of abiotic stress. While the important challenge of translation between controlled environment- and field-based experiments remains, the multiple revealed quantitative outputs from different abiotic stress conditions are genetically encoded. Consequently, the genetic explanations for these responses can now be elucidated using classical and molecular genetics. We propose this work as a time efficient method of dissecting the genetic mechanisms used by sorghum to respond to abiotic stress. In summary, this work provides a mechanism to overlay high throughput phenotyping with field studies to accelerate crop improvement.

AUTHOR SUMMARY

Sorghum is important for food security in developing countries and has potential as a high yielding biofuel crop. In either setting, the plant is likely to experience resource limited growing conditions. 'Resource use efficiency' and 'abiotic stress tolerance' are distinct biologically important phenotypes. The former refers to the ability of a crop to translate a provided resource, such as fertilizer or water, into yield. The latter refers to the ability of a crop to survive within resource limited environments. Here we describe and apply high-throughput phenotyping methods and element profiling to sorghum under abiotic stress conditions. We quantify abiotic stress responses of genetically diverse sorghum accessions based on color fluctuations, biomass accumulation, growth rate over time and elemental profile. Through this analysis we report 'resource use efficient' and 'abiotic stress tolerant' sorghum.

INTRODUCTION

The selection of efficient, stress-tolerant plants is essential for tackling the challenges of food security and climate change, particularly in hot, semiarid regions that are vulnerable to economic and environmental pressures (1–4). Many crop species, having undergone both natural and human selection, harbor abundant, untapped genetic diversity. This genetic diversity will be a valuable resource for selecting and breeding crops to maximize yield under adverse environmental conditions (5). Sorghum (*Sorghum bicolor* (L.) Moench) originated in northern Africa and was domesticated 8,000 – 10,000 years ago. Thousands of genotypes displaying a wide range of phenotypes have been collected and described (6–8). *Sorghum bicolor*, the primary species in cultivation today, has many desirable qualities including the ability to thrive in arid soils with minimal inputs, and many end-uses (9,10). For example, grain varieties are typically used for food and animal feed production, sweet sorghum genotypes accumulate non-structural, soluble sugar for use as syrup or fuel production, and bioenergy sorghum produces large quantities of structural, lignocellulosic biomass that may be valuable for fuel production (11,12). Sorghum genotypes can be differentiated and categorized by type according to these end-uses.

Rising interest in sorghum over the last forty years has led to efforts to preserve and curate its diversity. To maximize utility, these germplasm collections must now be characterized for performance across diverse environments (13–15). Deficits in our understanding of genotype-by-environment interactions (G x E = P, where G = genotype, E = environment and P = phenotype) are limiting current breeding efforts (16). Controlled-environment studies are quantitatively robust but are often viewed with skepticism regarding their translatability to field settings. Further, they can often accommodate only a limited number of genotypes at a time. In contrast, field level studies allow for large numbers of genotypes to be evaluated simultaneously. However, these studies provide limited resolution to resolve the effect of environment on phenotype and often require multi-year replication. This conundrum has motivated enthusiasm for both controlled environment and field level high throughput phenotyping platforms. However, the use of large-scale phenotyping and statistical modeling to predict field-based outcomes is challenging (17–19).

Here, we sought to define a set of measureable, environmentally-dependent phenotypic outputs to aid crop improvement. We utilize automated phenotyping techniques under controlled-environmental conditions to characterize G x E interactions on a diverse panel of sorghum genotypes in response to abiotic stress. We describe and quantify statistically robust differences among the genotypes to nutrient-poor conditions and drought stress. Using image analysis to characterize leaf color and biomass over time in conjunction with ionomics, we report measureable, genetically-encoded, phenotypic traits that are responsive to abiotic stress. This work provides a foundation for understanding the range of sorghum early-responses to abiotic stress and defines biologically important characteristics that can subsequently be investigated within field settings.

RESULTS

Phenotypic effects of abiotic stress on a sorghum diversity panel

Nitrogen and water availability are two of the most important environmental factors constraining plant productivity (20,21). For this study, sorghum was chosen for its genetic diversity and wide range of abilities to thrive under semi-arid, nutrient-limited

conditions. In order to test the role that genotype plays in response to environmental stress, a panel of 30 sorghum lines was assembled (Table S1). This panel includes sorghum accessions from all five cultivated races (bicolor, caudatum, durra, guinea and kafir), representing a variety of geographic origins and morphologies (22,23). The genotypes also display a range of photoperiod sensitivities and are categorized into three general production types: grain, sweet, and bioenergy. Figure 1 illustrates the overall experimental design to test the phenotypic effects of nitrogen deprivation and drought stress with two independent, three-week-long experiments using high-throughput phenotyping. For the nitrogen deprivation experiment, we chose to analyze the effect of the source (i.e. ammonium vs. nitrate) and quantity of nitrogen on sorghum development (Figure 1A, methods). Plants were watered daily with the indicated solution. For the drought stress experiment, we tested the effect of mild water deprivation and recovery from extreme drought (Figure 1B). Fertilizer nutrient concentrations were similar to what was included in the 50%/10% (NH_4^+/NO_3^-) nitrogen treatment, compensating for variable water volumes (see methods). Thus, the drought 70% and the nitrogen 50%/10% treatment groups are the most similar across the two experiments.

Figure 1. Experimental Overview. A, B) Watering regime used for nitrogen deprivation (A) and drought stress (B). The x-axis shows the age of the plants throughout the experiment and the y-axis indicates the estimated volume of water plus nutrients (ml), calculated based on the weight change of the pot before and after watering. Each dot represents the average amount of water delivered each day with vertical lines indicating error (99% confidence interval). Watering regime was increased due to plant age (shades of blue). The experimental treatments are listed above the plots. A) Volume of water and source of nitrogen is indicated and was scaled based on the 100% treatment group. Watering was kept constant between treatment groups B) Amount of water delivered was scaled based on the 100% treatment group (1 mM ammonium / 14.5 mM nitrate). Arrow indicates the end of extreme drought treatment and beginning of recovery. Nutrients were constant between treatment groups. C) Image analysis. From left to right: Example original RGB image taken from phenotyping system, plant isolation

mask generating using PlantCV, two examples of attributes analyzed (area and color). Scale bar = 15 cm.

All plants were photographed daily and images were processed using the open source PlantCV analysis software package ((24), http://plantcv.danforthcenter.org). Within each RGB image, the plant area was defined and isolated, allowing phenotypic attributes to be analyzed (Figure 1C). In total, 18 different shape characteristics were quantified (Figure S1). Principal component analysis (PCA) of all the quantified attributes revealed that shape characteristics could be used to separate treatments for both the nitrogen deprivation and the drought stress experiments (Figure 2A, B). Our results indicated that “area” was the plant shape feature that displayed the largest treatment affect (Figure 2A, B). Area measurements from plant images and biomass measurements have been shown to be correlated for a number of plant species, including sorghum (24,25). We also measured color attributes over time for the plants within both experiments. In contrast to shape, color attributes were only strongly altered by the lowest nitrogen treatment (Figure 2C). The effect of low nitrogen on plant color is well established and RGB image-based methods have been described to estimate chlorophyll content of leaves (26–31). Consequently, we focus on area and color to investigate genotypic differences in response to nitrogen deprivation and drought stress over time, though other shape attributes may prove to be useful for future analysis. To view the effect that our experimental treatments had on the measured shape characteristics and color for each individual genotype, an interactive version of the generated plant growth curves over time is available here: (http://shiny.bioinformatics.danforthcenter.org/Bart_Lab_Sorghum).

Figure 2. Determining plant attributes affected by experimental treatments. A) Left: Principle Component Analysis (PCA) plots of shape attributes for plants subjected to nitrogen deprivation (orange, green, purple) at the beginning and end of the experiment (plant age 8 days and 26 days). The shape attributes included in the PCA are as follows: area, hull area, solidity, perimeter, width, height, longest axis, center of mass X-axis, center of mass Y-axis, hull vertices, ellipse center x-axis, ellipse center Y-axis,

ellipse major axis, ellipse minor axis, ellipse angle and ellipse eccentricity. Right: Bar graph indicating measurability of shape attributes, showing the proportion of variance explained by treatment (i. e. treatment effect, y-axis) B) Similar to A, but for plants subjected to drought stress (red, blue, yellow). C) PCA plots showing analysis of color values within the mask for plants subjected to nitrogen deprivation (left) and drought stress (right) toward the beginning and the end of each experiment. All 360 degrees of the color wheel were included, binned every 2 degrees.

Nitrogen source and availability affect growth over time in a genotype-specific manner

Many factors contribute to the ability of plants to utilize nutrients and presumably, much of this is genetically explained. Correspondingly, genotype was a highly significant variable (*p*-value = 0.003 when measuring area) within the nitrogen deprivation analysis. To investigate how much nitrogen use efficiency is explained by major genotypic groupings, we calculated the contribution of type, photoperiod, or race on treatment affect. Photoperiod was the only other category that significantly contributed to biomass outcomes (Figure 3A, B). To identify sorghum varieties tolerant to growth in nutrient limited conditions, we considered end biomass within the most severe nitrogen deprivation treatment group for all genotypes (Figure 3C). China 17 and San Chi San are considered nitrogen-use-efficient genotypes, while BTx623 and CK60B are thought to be less efficient (32,33). We found China 17 and San Chi San to be better than the average of all other genotypes at acquiring biomass under low nitrogen conditions. Similarly, CK60B was slightly smaller than average. However, BTx623 was one of the higher biomass varieties in our experiment indicating limitations associated with this definition of nitrogen use efficiency. Growth chamber, greenhouse and field experiments are each advantageous and at the same time imperfect for distinct reasons. With this in mind, next we aimed to more fully capitalize on the specific advantage of expanded temporal resolution available from high throughput phenotyping platforms. For these experiments we considered average growth rate across the experiment (Figure 3D). Overall, end biomass measurements correlated well with overall growth rates. For example, by both measures, Della displayed particularly weak growth characteristics under low nitrogen conditions while BTx623 performed well. However, the correlation

was imperfect. San Chi San displayed the largest end biomass but was statistically average in terms of growth rate across the experiment. Discrepancies between end-biomass and growth rate (e.g. large plants with average or low observed growth rates) may indicate differences in germination rates (e.g. being larger at the beginning of the phenotyping experiment).

Figure 3. Growth response of genotypes to nitrogen deprivation. A) Tables showing results of ANOVA indicating significance of experimental variation explained by either genotype, type, photoperiod or race as found by Wald's Chi-Square tests with their associated degrees of freedom (DF). Significant *p*-value < 0.1, bold. All three nitrogen treatments are included in the calculations. B) Line graphs representing changes in plant area (y-axis) with age (x-axis) for all 30 sorghum genotypes examined. The experimental treatments are listed above the plots and genotypes have been separated by photoperiod sensitivity (legend, right). C and D) Graphs showing average end biomass (C, box plot (area), * *q*-values < 0.01) with outliers (colored dots), and growth rate (D, average change in area per day, days 10-22) for the 10/10 treatment group. The dotted lines indicate the treatment group average. Genotypes that displayed greater than average (blue) or less than average (magenta) growth are indicated. Error bars: 95% confidence intervals for both graphs.

To further explore nitrogen use efficiency, we factored timing of growth response into our analysis. For each day, we analyzed biomass for each genotype within the 100% control group (100 NH_4^+/100 NO_3^-) and compared that to the biomass within the 10% treatment group (10 NH_4^+/10 NO_3^-). Comparing these two populations allowed us to determine when, during the course of our experiment, those figures became significantly different (Figure 4A). This analysis separated the genotypes into two broad categories: "early" responding accessions and "late" responding accessions. Early- and late-responding lines were not found to be significantly different in terms of size before treatment administration (Figure 4B, top panel). Therefore, we hypothesized that either 1) lines would be late-responding because they were proficient at using any level of available nitrogen or 2) because they grew slowly regardless of quantity of nitrogen

supplied. We found that the early-responding lines were larger, on average, than the late-responding lines within the 100% treatment group (Figure 4B, bottom panel) suggesting that these lines are more competent at using available nitrogen. A subset of these genotypes are displayed in Figure 4C to illustrate our observations. The genotype Atlas is an example of a very early responding line, and it was one of the largest plants in the 100% treatment group, but also one of the worst-performing lines in the 10% treatment group (Figures 3C, 3D, 4C). In contrast, China 17 performed relatively well under nitrogen-limited conditions (10/10), but when nitrogen was abundant (100/100) the biomass accumulation was poor (Figure 3C, 3D, 4C). Taken together, these results point toward a potential inverse correlation between nitrogen use efficiency (defined as the ability to translate large quantities of nitrogen into biomass) and nitrogen deprivation tolerance (defined as ability to relatively thrive in low nitrogen conditions).

Figure 4. Timing of nitrogen deprivation response: size changes in late and early responding genotypes to nitrogen deprivation. A) Statistical analysis of differences in area over time (bottom, plant age) for the 30 sorghum genotypes analyzed. *q*-values for the heat map are indicated in blue, with darkest coloring representing most significance. The Canberra distance-based cluster dendrogram (right) was generated from calculated *q*-values. B) Box plots showing average biomass (area) with outliers (colored dots) for late- (left) and early- (right) responding lines from panel A at the beginning (day 8, top) and end (day 26, bottom) of the experiment. * p-value < 5×10^{-6}. C) Scatter plots representing plant area (y-axis) by treatment (x-axis) at the beginning (day 8), middle (day 19), and end (day 26) of the experiment for chosen late responding (left) and early responding (right) genotypes (key, right). Each dot represents an individual plant on a day and dotted lines connect genotypic averages. D and E) Color analysis (late responders, left; early responders, right) at day 14. Grey areas indicate standard error.

In addition to simply varying the amount of nitrogen available, we also tested whether any lines harbor a preference for nitrogen source. Nitrogen is typically available in two ionic forms within the soil, ammonium and nitrate, both of which are actively

taken up into plant roots by transporters located in the plasma membrane (34,35). Expression of these gene products and others have been shown to be responsive to nitrogen availability in sorghum (36). For example, San Chi San and China 17 are known to have higher levels of expression of nitrate transporters when compared to nitrogen-use-inefficient lines (33). Notably, San Chi San showed no change in average biomass when the ammonium levels were decreased from 50% to 10% while Atlas displayed the opposite response (Figure 4C). Among the 30 tested genotypes, 16 displayed little difference between the 50/10 and 10/10 groups in terms of biomass toward the end of the experiment (Figure S2). This highlights the importance of considering both quantity and source when investigating nitrogen use efficiency and points to yet another complexity surrounding our understanding of nitrogen use efficiency in plants.

In addition to affecting shape attributes, nitrogen starvation generally results in reduced chlorophyll content and increased chlorophyll catabolism. Other groups have used image analysis to estimate chlorophyll content and nitrogen use in rice (28). The RGB images contain plant hue channel information, and this was found to be a separable characteristic within our treatment groups (Figure 2C). We assessed color-based responses to nitrogen deprivation in the early- and late-responding genotypes as defined in Figure 4A. To facilitate this analysis we averaged the histograms of the chosen individuals within the early and late categories in each treatment group. We found that the histograms of the plant images contained two primary peaks: yellow and green. For both early- and late-responding lines, the yellow peak was larger and the green peak smaller for the plants in the 10% treatment group as compared to the 100% treatment group (Figure 5). Early responding lines within the 100% treatment group displayed the largest green-channel values. Late responding lines grown under nitrogen-limiting conditions displayed the largest yellow channel values (Figure 5, top row). In order to assign color-based treatment effects, we subtracted the 10% histograms from the 100% histograms and plotted this difference (Figure 5, bottom row). This revealed that although the late responding lines were more yellow, the magnitude difference from the treatment was similar for early and late lines in the yellow channel (Figures 5, S3). In contrast, the early-responding lines tended to have a larger green

channel difference between the 10% and the 100% treatment groups (Figure 5, S3), with early-responding lines showing a larger difference in the green channel. This analysis suggests that for nutrient-based studies known to affect chlorophyll accumulation, specifically nitrogen, color-based image analysis is consistent with and complimentary to the more-established biomass measures of fitness and performance.

Figure 5. Color changes in late and early responding genotypes to nitrogen deprivation. Top row: Average histograms illustrating percentage of identified plant image mask (y-axis) represented by a particular hue channel (x-axis). Presented is the average of the chosen early and late responding lines. Second row: Difference of histograms from top row. Grey areas indicate standard error.

Sorghum genotypes show a spectrum of drought tolerance over time

Sorghum is valued as a drought-tolerant C_4 grass (7). Just as nitrogen deprivation can manifest in many different ways, so can drought stress. To define relative drought tolerance among diverse sorghum varieties, we designed an experiment that would simultaneously test genotypic responses to mild drought as well as recovery from extreme water deprivation (Figure 1B). First we visualized the effects of mild drought on growth for the diversity panel of 30 genotypes (Figure 6A). In contrast to our analysis of nitrogen deprivation (Figure 3A), only genotype was a significantly contributing factor for biomass accumulation by drought treatment over time. Here again San Chi San accumulated the most biomass at the end of the experiment within the 70% treatment group (Figure 6B, C). However, growth rate measurements indicate that San Chi San was average to below average in terms of accumulation per day (Figure 6D). Thus, the large biomass measurement is likely the product of quick germination and/or growth during the first few days after germination. In contrast, accession PI_297155 was one of the lowest biomass-accumulating lines but showed a strikingly fast growth rate (Figure 6D). This particular genotype was very small at the beginning and displayed an accelerating growth rate toward the latter-half of the experimental timeframe (Figure 6B, Supplemental Shiny App

(shiny.bioinformatics.danforthcenter.org/Bart_Lab_Sorghum). These observations highlight the importance of a multi-pronged approach to describing plant phenotypes.

Figure 6. Growth response of genotypes to drought stress. A) Tables showing results of ANOVA indicating significance of experimental variation explained by either genotype, type, photoperiod or race as found by Wald's Chi-Square tests with their associated degrees of freedom (DF). Significant *p*-value < 0.1, bold. Only 100 and 70 drought treatments are included. B) Line graphs representing changes in plant size (log area, y-axis) with age (x-axis) for all 30 sorghum genotypes examined (key, right). The experimental treatments are listed above the plots. C) Graphs showing average end biomass (top, box plot (log area), * *q*-values < 0.01) with outliers (colored dots), and growth rate (bottom, average change in log area per day, days 10-22) for the 70% treatment group. The dotted lines indicate the treatment group average. Genotypes that displayed greater than average (blue) or less than average (magenta) growth are indicated. Error bars: 95% confidence intervals for both graphs.

To assess timing of response we used the biomass information for each genotype per day to look for when the 100% and 70% treatment groups became significantly different (Figure 7A). Using this method we found that the 30 genotypes separated into two distinct groups (early-responding and late-responding), though the *q*-value defining the difference in response timing between these groups was less significant than what was observed for the nitrogen deprivation experiment. This may indicate that the 70% watering regime was a relatively mild treatment as compared to the 50/10 nitrogen treatment, in terms of biological response. Contrary to what was seen for the nitrogen deprivation experiment, the average sizes of the early-and late-responding groups at the beginning of the experiment were measurably different (Figure 7B, top panel, T-test *p*-value = 0.00167). However, bootstrapping analysis failed to support a significant difference between the groups at day 8 (*p*-value 0.427). Therefore, we conclude that this difference in mean biomass at day 8 is unlikely to be biologically meaningful. At the end of the experiment, the early-responding lines were significantly larger than the late-responding lines, on average, in the 100% treatment group (Figure

353 7B, bottom panel). To illustrate our observations, we chose representative early- and
354 late-responding lines to display in Figure 7C. Within the late-responding lines, Della and
355 PI_655972 performed well in the 100% treatment group. Notably, these lines were
356 unremarkable among all 30 sorghum varieties when grown in the 70% treatment group
357 (Figure 6C, D). This observation suggests a possible tradeoff between water use
358 efficiency displayed in water sufficient conditions and tolerance to water limited
359 conditions. Finally, in contrast to what was seen for nitrogen deprivation, where color
360 was an informative metric by which to analyze plant response to treatment, color was
361 not a defining factor for any of the treatment groups within the drought experiment
362 (Figures 2B, 7D).
363
364 **Figure 7. Timing of response to mild drought stress: size and color changes in**
365 **late and early responding genotypes to drought.** A) Statistical analysis of differences
366 in log area at the population level over time (bottom, plant age) for the 30 sorghum
367 genotypes analyzed. *q*-values for the heat map are indicated in blue, with darkest
368 coloring representing most significance. The Canberra distance-based cluster
369 dendrogram (right) was generated from calculated *q*-values. B) Box plots showing
370 average biomass (area) with outliers (colored dots) for late- (left) and early- (right)
371 responding lines from panel A at the beginning (day 8, top) and end (day 26, bottom) of
372 the experiment. * *p*-value < 5×10^{-6}. C) Scatter plots representing plant area (y-axis) by
373 treatment (x-axis) at the beginning (day 8), middle (day 19), and end (day 26) of the
374 experiment for chosen late responding (left) and early responding (right) genotypes
375 (key, right). Each dot represents an individual plant on a day and dotted lines connect
376 genotypic averages. D) Difference of average histograms from chosen late-responding
377 and early-responding genotypes (14-day-old plants). Shown is the difference in the
378 percentage of identified plant image mask (y-axis) represented by a particular hue
379 channel (x-axis) between the 70% and 100% treatment groups. Grey areas indicate
380 standard error.
381
382 In addition to understanding sorghum response to mild drought, we aimed to
383 assess performance during, and recovery from, extreme drought. Within the 'recovery'

384 treatment plants received decreasing amounts of water for the first half of the
385 experiment followed by a recovery period equivalent to the 70% watering regime (Figure
386 1B, 6B). With this experiment we tested the hypothesis that some genotypes may be
387 able to endure temporary, extreme drought and later compensate with increased growth
388 rates when conditions improve. During the recovery period, the majority of sorghum
389 lines did not grow at a statistically different rate than those that had been maintained in
390 the 70% water treatment group (Figure 8). However, several genotypes (highlighted in
391 blue) grew significantly faster during recovery from extreme drought than the constant
392 70% treatment. This observation indicates that some sorghum varieties have evolved
393 mechanisms to survive extreme drought conditions and are further equipped to rapidly
394 take advantage of available resources when conditions improve.
395
396 **Figure 8. Rates of recovery from extreme drought treatment.** Shown are the
397 differences in growth rates (change in log area, y-axis) for all 30 sorghum genotypes
398 analyzed (x-axis) between the 70% watering regime and the recovery samples following
399 extreme drought treatment (days 21-24, figure 1B). The dotted line indicates the
400 average growth rate difference calculated between the two treatment populations, while
401 the average growth rate difference for each genotype is plotted (dots). Genotypes that
402 displayed significantly faster (blue) or slower (magenta) growth rates following extreme
403 drought are indicated, in addition to those that were not significantly affected (black).
404 Error bars: 95% confidence intervals.
405
406
407 <u>Ionomic profiling as a heritable, independent, measurable readout of abiotic stress</u>
408 <u>response.</u>
409 In addition to the image-based analysis used above to reveal measureable
410 biomass- and color-based outcomes in response to abiotic stress, we also sought
411 ionomic signatures of stress response in sorghum at the end of the experiments
412 (Figures S4, S5). This analysis had two objectives: 1) to validate the robustness and
413 reproducibility of our experimental design and 2) to further define the G x E effect on
414 sorghum subjected to either nitrogen deprivation or drought conditions (Figures 9, 10).

We were unable to include the recovery drought samples due to the small size of many of the genotypes at the end of the experiment. It has been established that both genetic and environmental factors and their interactions play a significant role in determining the plant ionome (37–42). Each element was modeled as a function of both genotype and treatment, and genotype was a significant factor for most elements in both nitrogen deprivation and drought stress experiments (Figures 9A, 10A).

Figure 9. Ionomic profiling of genotypes at the end of nitrogen deprivation treatments. A) Top Panel: A total variance partition model is created for every element and being shown is the percent variance explained by each partition of the model (yellow: genotype, green: treatment, purple: interaction between genotype and treatment, grey: unexplained variance). Bottom Panel: Significance of contribution from each partition is assessed using Wald's Chi-Square statistics. Significant cells (q-value < 0.05) are colored with levels of blue and non-significant cells are light grey. B) Top panel: Principal components are calculated over all elements, applied to the data and are color coded for treatment (left). 95% confidence ellipses are calculated for each of the treatment groups and the dots indicate the center of mass (right). The percent variance explained by each component is indicated in parenthesis. Bottom panel: Loadings for each element from the first two principal components are shown on the y-axis and are color filled based on the direction and strength of the contribution. Positive direction is colored blue and negative direction is colored red. For a given element, the color for PC1 and PC2 are related by the unit circle and saturation of the color is equal to the length of the projection into each of the two directions. C) Heat map by genotype testing the difference between the high (100/100) and low (10/10) treatment groups for every element using ANOVA. Significant cells (q-value < 0.05) are colored with levels of blue while non-significant cells are light grey.

Figure 10. Ionomic profiling of genotypes after mild drought stress. A) A total variance partition model is created for every element and being shown is the percent variance explained by each partition of the model (yellow: genotype, green: treatment, purple: interaction between genotype and treatment, grey: unexplained variance). B)

Top panel: Principal components are calculated over all elements, applied to the data and are color coded for treatment (left). 95% confidence ellipses are calculated for each of the treatment groups and the dots indicate the center of mass (right). The percent variance explained by each component is indicated in parenthesis. Bottom panel: Loadings for each element from the first two principal components are shown on the y-axis and are color filled based on the direction and strength of the contribution. Positive direction is colored blue and negative direction is colored red. For a given element, the color for PC1 and PC2 are related by the unit circle and saturation of the color is equal to the length of the projection into each of the two directions. C) Scatter plot showing percent contribution of genotype effect for each element (key: right) in both experiments (x-axis: nitrogen y-axis: drought). Solid black line represents linear best fit. R^2 shown in upper-left corner.

Nitrogen deprivation had a measurable effect on every element (Figures 9A, B) while a treatment effect could not be resolved between 100% and 70% water availability for most elements (Figure 10A). PCA of the elements revealed more separation of the nitrogen deprivation treatments than the drought treatments, with the two lower nitrogen treatment groups separating from the high treatment group (Figures 9B, 10B). Both micro (Se, Rb, Mo, Cd) and macro (K, P) nutrients contributed strongly to the PCs separating the 100/100 treatment group away from the other two treatments within the PCA (Figure 9B, bottom panel). Using the change in each element between the 100/100 and 10/10 as the response variable we clustered the accessions (Figures 9C). These groupings did not correlate with the observed biomass differences discussed above (Figure 4A, 7A, S6) indicating that the ionomic profile reflects different physiological properties. Together, these observations provide a baseline for further investigation into the role of the ionome in abiotic stress and the effect of abiotic stress on the ionome.

DISCUSSION

Crops adapted to nutrient-poor conditions will be an invaluable resource for realizing the goal of dedicated bioenergy crops grown without irrigation and limited

fertilizer on marginal lands. Robust, quantitative phenotypes are a prerequisite for genetic investigations and these can be gathered using high throughput phenotyping and image analysis. In order to test for and quantify G x E interactions we designed a strategy that utilized tightly controlled environmental conditions in a high-throughput manner in the genetically diverse, stress-resistant crop, sorghum. Responding to stress is costly to plants. As such, there may be inherent trade-offs associated with ability to thrive under multiple abiotic stress conditions. Overall our results indicate that no single variety is optimized for both abiotic stresses tested in terms of biomass accumulation. Within this context, we went beyond characterizing biomass as an output of stress tolerance and measured changes in color and elemental profile. This work highlights the fact that the generally observed and measured response to a given abiotic stress may often appear to be the same (i. e. stressed plants produce less biomass), but the biological and chemical signaling within the plant is distinct depending on the stress. These signals and responses are much more difficult to measure, but will be critical for understanding and improving plant resistance to abiotic stress going forward.

Previous work has shown that plants can utilize different forms of nitrogen, yet preference can be influenced greatly by genotype and the environment (35). Factors such as soil pH, CO_2 levels, temperature and the availability of other nutrients have an impact on nitrogen uptake (43,44). Ammonium causes acidification of the soil, which affects the uptake of other nutrients and likely alters the root microbiome. Additionally, root architecture is affected by nitrogen source and nutrient availability. It has been shown for a number of species, including maize and barley, that ammonium causes a reduction in lateral root branching that can be reversed with the addition of phosphorous (45,46,42,47). In *Arabidopsis*, nitrogen-phosphorous signaling has been studied in detail and the presence of nitrate has been shown to inhibit phosphorous uptake (48,49). We measured the effects of nitrogen deprivation as well as the source of nitrogen (ammonium vs nitrate). Some genotypes were more affected by nitrogen source in terms of end biomass than others, for example the difference between San Chi San and Atlas (Figure 4C). Through ionomic profiling after the nitrogen deprivation experiment, we show that phosphorous was one of the elements with the largest treatment effect

(Figures 9). Dry weight-based concentration of phosphorous was higher in the low nitrogen treatment groups, both of which received the same nitrate treatment, compared to the high nitrogen treatment group (Figure S4). This highlights the value of tightly controlled environments for elucidating the possible conservation and nuances of plant growth responses. Taken together, these data are consistent with what other studies that have shown: some genotypes have a preference for nitrogen source and other environmental factors influence that preference.

Some of the most productive crops in use today are C4 grasses like corn (*Zea mays*), sorghum (*Sorghum bicolor*), and sugarcane (primarily *Saccharum officinarum*) (Reviewed in Leakey, 2009). These crops have cellular functions and chemistries that result in high rates of photosynthesis in spite of drought and nutrient-poor conditions. However, within each crop group, significant genetic and phenotypic variety exists. The sorghum diversity panel presented here represents a wide, yet incomplete, range of known sorghum genotypic and phenotypic diversity. Tens of thousands of sorghum accessions are curated and maintained by a number of national and international institutions (22). The largest such institution, the US National Sorghum Collection (GRIN database), provides agronomic characteristic information for 40–60 % of the collection (e. g. growth and morphology characteristics, insect and disease resistance, chemical properties, production quality, photoperiod in temperate climates). Thus, much work is yet to be done to fully characterize and maximize the potential of this hearty, productive crop species.

Nitrogen and water use efficiency are traditionally defined by the difference in biomass between plants grown in resource sufficient versus resource limited conditions at the end of the growing season. Stated differently, this measure asks the question: How efficient is a plant at translating a provided resource (nitrogen or water) into plant biomass. Equally important is the ability to efficiently use a limited resource. Factors that play into these distinct definitions of resource use efficiency include ability to survive periods of extreme stress and rapid utilization of resources as they become available. In this manuscript, we make progress toward deconstructing the building blocks that make

539 up nitrogen and water use efficiency phenotypes. These analyses reveal diverse
540 quantitative indicators of abiotic stress and genotypic differences in stress mitigation.
541 Having deconstructed these building blocks, we are now in a position to discover the
542 underlying genetic explanations for genotypic variability in resource use efficiency and
543 tolerance to resource limited growth conditions. Further, this work forms a foundation for
544 future research to overlay additional abiotic and biotic stress conditions to achieve a
545 holistic view of sorghum G x E phenotypes. The overall goal of this research is to
546 support such efforts and expedite the process of meaningful crop improvement.
547

548 **MATERIALS AND METHODS**

549 Plant growth conditions

550 Round pots (10 cm diameter) fitted with drainage trays were pre-filled with Profile® Field
551 & Fairway™ calcined clay mixture (Hummert International, Earth City, Missouri) the goal
552 being to minimize soil contaminates (microbes, nutrients, etc.) and maximize drainage.
553 Before the beginning of each experiment, the thirty genotypes of *Sorghum bicolor* (L.)
554 Moench (Table S1) were planted, bottom-watered once daily using distilled water
555 (reverse osmosis), then allowed to germinate for 6 days in a Conviron growth chamber
556 (day/night temperature: 32ºC/22ºC, day/night humidity: 40%/50% (night), day length:
557 16hr, light source: Philips T5 High Output fluorescent bulbs (4100 K (Cool white)) and
558 halogen incandescent bulbs (2900K (Warm white)), light intensity: 400 µmol/m^2/s). On
559 day 6, plants were barcoded (including genotype identification, water treatment group,
560 and a unique pot identification number), randomized, then loaded onto the Bellwether
561 Phenotyping Platform (Conviron, day/night temperature: 32ºC/22ºC, day/night humidity:
562 40%/50% (night), day length: 16hr, light source: metal halide and high pressure sodium,
563 light intensity: 400 µmol/m^2/s) Plants continued to be watered using distilled water by
564 the system for another 2 days, with experimental treatments (described below) and
565 imaging beginning on day 8.
566

567 Nitrogen deprivation treatments:

568 (100% Ammonium/100% Nitrate): 6.5 mM KNO_3, 4.0 mM $Ca(NO_3)_2 \cdot 4H_2O$, 1.0 mM
569 $NH_4H_2PO_4$, 2.0 mM $MgSO_4 \cdot 7H_2O$, micronutrients, pH ~4.6

(50% Ammonium/10% Nitrate): 0.65 mM KNO_3, 4.95 mM KCl, 0.4 mM $Ca(NO_3)_2{\cdot}4H_2O$, 3.6 mM $CaCl_2{\cdot}2H_2O$, 0.5 mM $NH_4H_2PO_4$, 0.5 mM KH_2PO_4, 2.0 mM $MgSO_4{\cdot}7H_2O$, pH ~4.8

(10% Ammonium/10% Nitrate): 0.65 mM KNO_3, 4.95 mM KCl, 0.4 mM $Ca(NO_3)_2{\cdot}4H_2O$, 3.6 mM $CaCl_2{\cdot}2H_2O$, 0.1 mM $NH_4H_2PO_4$, 0.9 mM KH_2PO_4, 2.0 mM $MgSO_4{\cdot}7H_2O$, micronutrients, pH ~5.0

The same micronutrients were used for all above treatments: 4.6 µM H_3BO_3, 0.5 µM $MnCl_2{\cdot}4H_2O$, 0.2 µM $ZnSO_4{\cdot}7H_2O$, 0.1 µM $(NH_4)_6Mo_7O_{24}{\cdot}4H_2O$, 0.2 µM $MnSO_4{\cdot}H_2O$, 71.4 µM Fe-EDTA

Drought stress treatments: concentrations of macro- and micronutrients adjusted for volume delivered, based on formulation used in 50% Ammonium/10% Nitrate treatment above.

100% (same as 50% Ammonium/10% Nitrate): 0.65 mM KNO_3, 4.95 mM KCl, 0.4 mM $Ca(NO_3)_2{\cdot}4H_2O$, 3.6 mM $CaCl_2{\cdot}2H_2O$, 0.5 mM $NH_4H_2PO_4$, 0.5 mM KH_2PO_4, 2.0 mM $MgSO_4{\cdot}7H_2O$, 4.6 µM H_3BO_3, 0.5 µM $MnCl_2{\cdot}4H_2O$, 0.2 µM $ZnSO_4{\cdot}7H_2O$, 0.1 µM $(NH_4)_6Mo_7O_{24}{\cdot}4H_2O$, 0.2 µM $MnSO_4{\cdot}H_2O$, 71.4 µM Fe-EDTA, pH ~4.8

70% (days 8-26) and Recovery (days 19-26): 0.93 mM KNO_3, 7.07 mM KCl, 0.57 mM $Ca(NO_3)_2{\cdot}4H_2O$, 5.14 mM $CaCl_2{\cdot}2H_2O$, 0.71 mM $NH_4H_2PO_4$, 0.71 mM KH_2PO_4, 2.86 mM $MgSO_4{\cdot}7H_2O$, 6.57 µM H_3BO_3, 0.71 µM $MnCl_2{\cdot}4H_2O$, 0.29 µM $ZnSO_4{\cdot}7H_2O$, 0.14 µM $(NH_4)_6Mo_7O_{24}{\cdot}4H_2O$, 0.29 µM $MnSO_4{\cdot}H_2O$, 102 µM Fe-EDTA, pH ~4.7

Recovery (days 8-18): 1.3 mM KNO_3, 9.9 mM KCl, 0.8 mM $Ca(NO_3)_2{\cdot}4H_2O$, 7.2 mM $CaCl_2{\cdot}2H_2O$, 1.0 mM $NH_4H_2PO_4$, 1.0 mM KH_2PO_4, 4 mM $MgSO_4{\cdot}7H_2O$, 9.2 µM H_3BO_3, 1.0 µM $MnCl_2{\cdot}4H_2O$, 0.4 µM $ZnSO_4{\cdot}7H_2O$, 0.2 µM $(NH_4)_6Mo_7O_{24}{\cdot}4H_2O$, 0.4 µM $MnSO_4{\cdot}H_2O$, 142.8 µM Fe-EDTA, pH ~4.5

Image Processing

Images were analyzed by using an open-source platform named PlantCV. This package primarily contains wrapper functions around the commonly used open-source image analysis software called OpenCV. To get useful information from a given image, the plant must be segmented out of the picture using various mask generation methods to remove the background so all that remains is plant material (see figure 1). A pipeline was developed to complete this task for the side-view and top-view cameras separately and they were simply repeated for every respective image in a high-throughput computation cluster. For this dataset of approximately 90,000 images with the computation split over 40 cores, computation time was roughly four hours. Upon completion, data files are created that contain parameterizations of various shape features and color information from several color-spaces for every image analyzed.

Outlier Detection and Removal Criteria

Outliers were detected and removed by implementing Cook's distance on a linear model (50) that only included the interaction effect of treatment, genotype and time. That is, for each observation, an influence measure is obtained as the difference of the model with and without the observation. After getting a measure for all observations in the dataset, outliers were defined as having an influence greater than four times that of the mean influence and were subsequently removed from the remaining analysis.

Bootstrap Methods

To better understand the importance of the difference between the two responder types, an empirical distribution is created by randomly selecting 10 genotypes to be in one group, placing the remaining 20 to be in the other, and calculating the difference in mean biomass between them. This process is repeated 1000 times and the p-value is calculated as the number of times the absolute value of the difference is greater than the difference of the early and late responders divided by 1000.

Exploratory PCA

Two types of PCA's are generated: one for the shape features and the other for color features. To get an idea of what shapes are important to examine further, all shape parameterizations that are generated from PlantCV are included in the dimensional reduction. Plotting PC1 vs PC2 shows that there is a separation of treatment groups along the PC1 axis in both drought and nitrogen experiments. Examining the eigenvalues and correlations for this axis shows the most important traits to be hull area, area, height, and perimeter and that these four traits are all highly correlated with each other. This observation is true in both experiments and the choice of using area for the primary outcome is two-fold. The first is that it is the trait that explains the most variance along PC1 and the second is that, relative to the other measures, area is the most robust to outlier pixels from image processing.

Along with the shape features, color as defined by the hue channel is examined with principal components. The hue channel is returned from PlantCV as the number of pixels in the image mask for a particular degree range of the hue spectrum. The resolution of color is within two degrees meaning that the hue circle, which is understood to be continuous, is broken up in two degree increments resulting in one hundred eighty bins and all of these bins are included in the dimensional reduction. While color does not appear to separate the treatment groups in the drought experiment, examining the eigenvalues of PC1 in the nitrogen experiment reveals that the degrees that correspond to yellow-like and green-like colors are the bins that are influencing the separation of the treatments.

Trends GLMM-ANOVA

Using area as the primary outcome, a general linear mixed model was created to identify significance sources of variance adjusting for all other sources, otherwise known as type III sum of squares. Designating genotype as G, treatment as E, and time as T, there are six fixed effects: G, E, GxE, GxT, ExT, GxExT. The mixed effect is a random slope and intercept of the repeated measures over time. To get a p-value for each source of variation, Wald Chi-Square statistic was implemented and is a leave-one-out model fitting procedure which allows for adjustment of all other sources.

663 Each Day GLM

664 Given that the ANOVA showed significance in the three-way interaction, is should be
665 true that there is variance in how long it took for a given genotype to respond. The
666 procedure was to simply loop through each genotype and each day and fit a linear
667 model that only includes the treatment effect. The p-value is obtained from a F-statistic
668 generated from the sum of squares of the treatment source of variation. After getting all
669 the raw p-values, a Benjamini-Hochberg FDR multiple comparisons correction is done
670 to aid in eliminating false positives. After the correction, there exists a small number of
671 p-values that are extremely small and a linear color gradient would be uninformative so
672 a log-transform of the q-values helps create a smoother, more informative, gradient.
673 A hierarchical-agglomeric clustering routine is done on the corrected p-values to bring
674 clusters within the data to light. Each line had an associated vector of p-values and a
675 Canberra distance is calculated for all pairwise vectors which are then grouped by
676 Ward's minimum variance method.
677
678 Color Processing
679 PlantCV returns several color-space histograms for every image that is run through the
680 pipeline (RGB, HSV, LAB, and NIR). Every channel from each color-space is a vector
681 representing values (or bins) from 0 to 255 which are black to full color respectively. All
682 image channel histograms were normalized by dividing each of the bins by the total
683 number of pixels in the image mask ultimately returning the percentage of pixels in the
684 mask that take on the value of that bin. The hue channel is a 360 degree
685 parameterization of the visible light spectrum and contains the number of pixels found at
686 each degree. The colors of most importance are between 0 and 120 degrees which
687 correspond to the gradient of reds to oranges to yellows to greens. Colors beyond this
688 range, like cyan and magenta, have values of all zeros and are not shown. Means and
689 95% confidence intervals as calculated on a per degree basis over the replicates.
690
691 Ionomics Profiling and Analysis
692 The most recent mature leaf was sampled from each plant on day 26 of each
693 experiment, placed in a coin envelope and dried in a 45ºC oven for a minimum of 48

hours. Large samples were crushed by hand and subsampled to 75mg. Subsamples or whole leaves of smaller samples were weighed into borosilicate glass test tubes and digested in 2.5 mL nitric acid (AR select, Macron) containing 20ppb indium as a sample preparation internal standard. Digestion was carried out by soaking overnight at room temperature and then heating to 95ºC for 4hrs. After cooling, samples were diluted to 10 mL using ultra-pure water (UPW, Millipore Milli-Q). Samples were diluted an additional 5x with UPW containing yttrium as an instrument internal standard using an ESI prepFAST autodilution system (Elemental Scientific). A Perkin Elmer NexION 350D with helium mode enabled for improved removal of spectral interferences was used to measure concentrations of B, Na, Mg, Al, P, S K, Ca, Mn, Fe, Co, Ni, Cu, Zn, As, Se, Rb, Mo, and Cd. Instrument reported concentrations are corrected for the yttrium and indium internal standards and a matrix matched control (pooled leaf digestate) as described (51). The control was run every 10 samples to correct for element-specific instrument drift. Concentrations were converted to parts-per-million (mg analyte/kg sample) by dividing instrument reported concentrations by the sample weight.

Due to low analyte concentrations, data from samples with less than 20 mg of tissue were removed from further analysis. This left very few samples in the 50% field capacity drought treatment, so this entire treatment was removed from further elemental analysis. Outliers were identified by analyzing the variance of the replicate measurements for each line in a treatment group and excluding a measurement from further analysis if the median absolute deviation (MAD) was greater than 6.2 (52).

ACKNOWLEDGEMENTS

We acknowledge Mindy Darnell and Leonardo Chavez from The Bellwether Foundation Phenotyping core facility at the Danforth center as well as Diana Fasanello and Molly Kuhs for their assistance in running the experiments. We would also like to thank Dr. Greg Ziegler for his help with the ionomics analysis and Dr. Stephen Kresovich for his many helpful discussions and for supplying the seed for the sorghum diversity panel.

REFERENCES

1. Lobell DB, Burke MB, Tebaldi C, Mastrandrea MD, Falcon WP, Naylor RL. Prioritizing Climate Change Adaptation Needs for Food Security in 2030. Science. 2008 Feb 1;319(5863):607–10.

2. Foley JA, Ramankutty N, Brauman KA, Cassidy ES, Gerber JS, Johnston M, et al. Solutions for a cultivated planet. Nature. 2011 Oct 20;478(7369):337–42.

3. DeLucia EH, Gomez-Casanovas N, Greenberg JA, Hudiburg TW, Kantola IB, Long SP, et al. The Theoretical Limit to Plant Productivity. Environ Sci Technol. 2014 Aug 19;48(16):9471–7.

4. Hadebe ST, Modi AT, Mabhaudhi T. Drought Tolerance and Water Use of Cereal Crops: A Focus on Sorghum as a Food Security Crop in Sub-Saharan Africa. J Agron Crop Sci [Internet]. 2016; Available from: http://dx.doi.org/10.1111/jac.12191

5. Leakey ADB. Rising atmospheric carbon dioxide concentration and the future of C4 crops for food and fuel. Proc R Soc Lond B Biol Sci. 2009 Jul 7;276(1666):2333–43.

6. Deu M, Rattunde F, Chantereau J. A global view of genetic diversity in cultivated sorghums using a core collection. Genome. 2006 Feb 1;49(2):168–80.

7. Paterson AH, Bowers JE, Bruggmann R, Dubchak I, Grimwood J, Gundlach H, et al. The Sorghum bicolor genome and the diversification of grasses. Nature. 2009 Jan 29;457(7229):551–6.

8. Lasky JR, Upadhyaya HD, Ramu P, Deshpande S, Hash CT, Bonnette J, et al. Genome-environment associations in sorghum landraces predict adaptive traits. Sci Adv [Internet]. 2015 Jul [cited 2017 Jan 9];1(6). Available from: https://www.ncbi.nlm.nih.gov/pmc/articles/PMC4646766/

9. Morris GP, Ramu P, Deshpande SP, Hash CT, Shah T, Upadhyaya HD, et al. Population genomic and genome-wide association studies of agroclimatic traits in sorghum. Proc Natl Acad Sci. 2013 Jan 8;110(2):453–8.

10. Vermerris W, Saballos A. Genetic Enhancement of Sorghum for Biomass Utilization. In: Paterson AH, editor. Genomics of the Saccharinae [Internet]. New York, NY: Springer New York; 2013. p. 391–425. Available from: http://dx.doi.org/10.1007/978-1-4419-5947-8_17

11. Murray SC. Differentiation of Seed, Sugar, and Biomass-Producing Genotypes in Saccharinae Species. In: Paterson AH, editor. Genomics of the Saccharinae [Internet]. New York, NY: Springer New York; 2013. p. 479–502. Available from: http://dx.doi.org/10.1007/978-1-4419-5947-8_20

12. Rooney WL. Sorghum. In: Karlen DL, editor. Cellulosic Energy Cropping Systems [Internet]. John Wiley & Sons, Ltd; 2014 [cited 2017 Jan 10]. p. 109–29. Available from: http://onlinelibrary.wiley.com.libproxy.wustl.edu/doi/10.1002/9781118676332.ch7/summary

13. Furbank RT, Tester M. Phenomics – technologies to relieve the phenotyping bottleneck. Trends Plant Sci. 2011 Dec;16(12):635–44.

14. Fiorani F, Schurr U. Future Scenarios for Plant Phenotyping. Annu Rev Plant Biol. 2013 Apr 29;64(1):267–91.

759 15. Araus JL, Cairns JE. Field high-throughput phenotyping: the new crop breeding frontier. Trends
760 Plant Sci. 2014 Jan;19(1):52–61.

761 16. Zamir D. Where Have All the Crop Phenotypes Gone? PLOS Biol. 2013 Jun 25;11(6):e1001595.

762 17. Deans AR, Lewis SE, Huala E, Anzaldo SS, Ashburner M, Balhoff JP, et al. Finding Our Way through
763 Phenotypes. PLOS Biol. 2015 Jan 6;13(1):e1002033.

764 18. Lipka AE, Kandianis CB, Hudson ME, Yu J, Drnevich J, Bradbury PJ, et al. From association to
765 prediction: statistical methods for the dissection and selection of complex traits in plants. Curr
766 Opin Plant Biol. 2015 Apr;24:110–8.

767 19. Zivy M, Wienkoop S, Renaut J, Pinheiro C, Goulas E, Carpentier S. The quest for tolerant varieties:
768 the importance of integrating “omics” techniques to phenotyping. Front Plant Sci [Internet]. 2015
769 [cited 2017 Apr 12];6. Available from:
770 http://journal.frontiersin.org/article/10.3389/fpls.2015.00448/abstract

771 20. Chapin FS, Bloom AJ, Field CB, Waring RH. Plant Responses to Multiple Environmental Factors.
772 BioScience. 1987;37(1):49–57.

773 21. Liu Q, Zhang Y, Yu N, Bi Z, Zhu A, Zhan X, et al. Genome sequence of Pseudomonas parafulva
774 CRS01-1, an antagonistic bacterium isolated from rice field. J Biotechnol. 2015 Jul 20;206:89–90.

775 22. Kimber CT, Dahlberg JA, Kresovich S. The Gene Pool of Sorghum bicolor and Its Improvement. In:
776 Paterson AH, editor. Genomics of the Saccharinae [Internet]. New York, NY: Springer New York;
777 2013. p. 23–41. Available from: http://dx.doi.org/10.1007/978-1-4419-5947-8_2

778 23. Brenton ZW, Cooper EA, Myers MT, Boyles RE, Shakoor N, Zielinski KJ, et al. A Genomic Resource
779 for the Development, Improvement, and Exploitation of Sorghum for Bioenergy. Genetics. 2016
780 Sep 1;204(1):21–33.

781 24. Fahlgren N, Feldman M, Gehan MA, Wilson MS, Shyu C, Bryant DW, et al. A Versatile Phenotyping
782 System and Analytics Platform Reveals Diverse Temporal Responses to Water Availability in
783 Setaria. Mol Plant. 2015 Oct;8(10):1520–35.

784 25. Neilson EH, Edwards AM, Blomstedt CK, Berger B, Moller BL, Gleadow RM. Utilization of a high-
785 throughput shoot imaging system to examine the dynamic phenotypic responses of a C4 cereal
786 crop plant to nitrogen and water deficiency over time. J Exp Bot. 2015 Apr 1;66(7):1817–32.

787 26. Hu H, Liu H, Zhang H, Zhu J, Yao X, Zhang X, et al. Assessment of Chlorophyll Content Based on
788 Image Color Analysis, Comparison with SPAD-502. In IEEE; 2010 [cited 2017 Feb 17]. p. 1–3.
789 Available from: http://ieeexplore.ieee.org/document/5678413/

790 27. Shibghatallah MAH, Khotimah SN, Suhandono S, Viridi S, Kesuma T, Joni IM, et al. Measuring leaf
791 chlorophyll concentration from its color: A way in monitoring environment change to plantations.
792 In: AIP Conference Proceedings [Internet]. AIP; 2013 [cited 2017 Feb 17]. p. 210–213. Available
793 from: http://aip.scitation.org/doi/abs/10.1063/1.4820322

794 28. Wang Y, Wang D, Shi P, Omasa K. Estimating rice chlorophyll content and leaf nitrogen
795 concentration with a digital still color camera under natural light. Plant Methods. 2014;10:36.

796 29. Cendrero-Mateo MP, Moran MS, Papuga SA, Thorp KR, Alonso L, Moreno J, et al. Plant chlorophyll
797 fluorescence: active and passive measurements at canopy and leaf scales with different nitrogen
798 treatments. J Exp Bot. 2016 Jan 1;67(1):275–86.

799 30. Junker LV, Ensminger I. Relationship between leaf optical properties, chlorophyll fluorescence and
800 pigment changes in senescing Acer saccharum leaves. Tree Physiol. 2016 Jun 1;36(6):694–711.

801 31. Mishra KB, Mishra A, Novotná K, Rapantová B, Hodaňová P, Urban O, et al. Chlorophyll a
802 fluorescence, under half of the adaptive growth-irradiance, for high-throughput sensing of leaf-
803 water deficit in Arabidopsis thaliana accessions. Plant Methods. 2016;12:46.

804 32. Maranville JW, Madhavan S. Physiological adaptations for nitrogen use efficiency in sorghum. In:
805 Food Security in Nutrient-Stressed Environments: Exploiting Plants' Genetic Capabilities [Internet].
806 Springer; 2002 [cited 2017 Feb 6]. p. 81–90. Available from:
807 http://link.springer.com/chapter/10.1007/978-94-017-1570-6_10

808 33. Gelli M, Duo Y, Konda AR, Zhang C, Holding D, Dweikat I. Identification of differentially expressed
809 genes between sorghum genotypes with contrasting nitrogen stress tolerance by genome-wide
810 transcriptional profiling. BMC Genomics. 2014;15(1):1.

811 34. Crawford NM, Forde BG. Molecular and Developmental Biology of Inorganic Nitrogen Nutrition.
812 Arab Book Am Soc Plant Biol [Internet]. 2002 Mar 27 [cited 2017 Feb 2];1. Available from:
813 http://www.ncbi.nlm.nih.gov/pmc/articles/PMC3243300/

814 35. Kiba T, Krapp A. Plant Nitrogen Acquisition Under Low Availability: Regulation of Uptake and Root
815 Architecture. Plant Cell Physiol. 2016 Apr 1;57(4):707–14.

816 36. Vidal EA, Moyano TC, Canales J, Gutiérrez RA. Nitrogen control of developmental phase transitions
817 in Arabidopsis thaliana. J Exp Bot. 2014 Oct 1;65(19):5611–8.

818 37. Baxter IR, Vitek O, Lahner B, Muthukumar B, Borghi M, Morrissey J, et al. The leaf ionome as a
819 multivariable system to detect a plant's physiological status. Proc Natl Acad Sci. 2008 Aug
820 19;105(33):12081–6.

821 38. Baxter I, Dilkes BP. Elemental Profiles Reflect Plant Adaptations to the Environment. Science. 2012
822 Jun 29;336(6089):1661–3.

823 39. Chao D-Y, Silva A, Baxter I, Huang YS, Nordborg M, Danku J, et al. Genome-Wide Association
824 Studies Identify Heavy Metal ATPase3 as the Primary Determinant of Natural Variation in Leaf
825 Cadmium in Arabidopsis thaliana. PLOS Genet. 2012 Sep 6;8(9):e1002923.

826 40. Asaro A, Ziegler G, Ziyomo C, Hoekenga OA, Dilkes BP, Baxter I. The Interaction of Genotype and
827 Environment Determines Variation in the Maize Kernel Ionome. G3 Genes Genomes Genet. 2016
828 Dec 1;6(12):4175–83.

41. Shakoor N, Ziegler G, Dilkes BP, Brenton Z, Boyles R, Connolly EL, et al. Integration of Experiments across Diverse Environments Identifies the Genetic Determinants of Variation in Sorghum bicolor Seed Element Composition. Plant Physiol. 2016 Apr 1;170(4):1989–98.

42. Thomas CL, Alcock TD, Graham NS, Hayden R, Matterson S, Wilson L, et al. Root morphology and seed and leaf ionomic traits in a Brassica napus L. diversity panel show wide phenotypic variation and are characteristic of crop habit. BMC Plant Biol [Internet]. 2016 Dec [cited 2017 Apr 12];16(1). Available from: http://bmcplantbiol.biomedcentral.com/articles/10.1186/s12870-016-0902-5

43. Jackson RB, Reynolds HL. Nitrate and ammonium uptake for single-and mixed-species communities grown at elevated CO2. Oecologia. 1996 Jan 1;105(1):74–80.

44. Coskun D, Britto DT, Kronzucker HJ. The nitrogen–potassium intersection: membranes, metabolism, and mechanism. Plant Cell Amp Environ [Internet]. 2016 Jan 1 [cited 2017 Apr 21]; Available from: http://onlinelibrary.wiley.com.libproxy.wustl.edu/doi/10.1111/pce.12671/full

45. Drew MC. Comparison of the effects of a localised supply of phosphate, nitrate, ammonium and potassium on the growth of the seminal root system, and the shoot, in barley. New Phytol. 1975;75(3):479–490.

46. Ma Q, Zhang F, Rengel Z, Shen J. Localized application of NH4+-N plus P at the seedling and later growth stages enhances nutrient uptake and maize yield by inducing lateral root proliferation. Plant Soil. 2013 Nov 1;372(1–2):65–80.

47. Giles CD, Brown LK, Adu MO, Mezeli MM, Sandral GA, Simpson RJ, et al. Response-based selection of barley cultivars and legume species for complementarity: Root morphology and exudation in relation to nutrient source. Plant Sci. 2017 Feb;255:12–28.

48. Kant S, Peng M, Rothstein SJ. Genetic Regulation by NLA and MicroRNA827 for Maintaining Nitrate-Dependent Phosphate Homeostasis in Arabidopsis. PLOS Genet. 2011 Mar 24;7(3):e1002021.

49. Lin W-Y, Huang T-K, Chiou T-J. NITROGEN LIMITATION ADAPTATION, a Target of MicroRNA827, Mediates Degradation of Plasma Membrane-Localized Phosphate Transporters to Maintain Phosphate Homeostasis in Arabidopsis. Plant Cell. 2013 Oct 1;25(10):4061–74.

50. Cook RD. Detection of influential observation in linear regression. Technometrics. 1977;19(1):15–18.

51. Ziegler G, Terauchi A, Becker A, Armstrong P, Hudson K, Baxter I. Ionomic Screening of Field-Grown Soybean Identifies Mutants with Altered Seed Elemental Composition. Plant Genome. 2013;6(2):0.

52. Davies L, Gather U. The Identification of Multiple Outliers. J Am Stat Assoc. 1993 Sep 1;88(423):782–92.

Supplemental raw data files:

sorg_nitrogen_all_shapes.csv

sorg_nitrogen_all_colors.csv

sorg_drought_all_shapes.csv

sorg_drought_all_colors.csv

Ionomics_RawData_Nitrogen.csv

Ionomics_RawData_Drought.csv

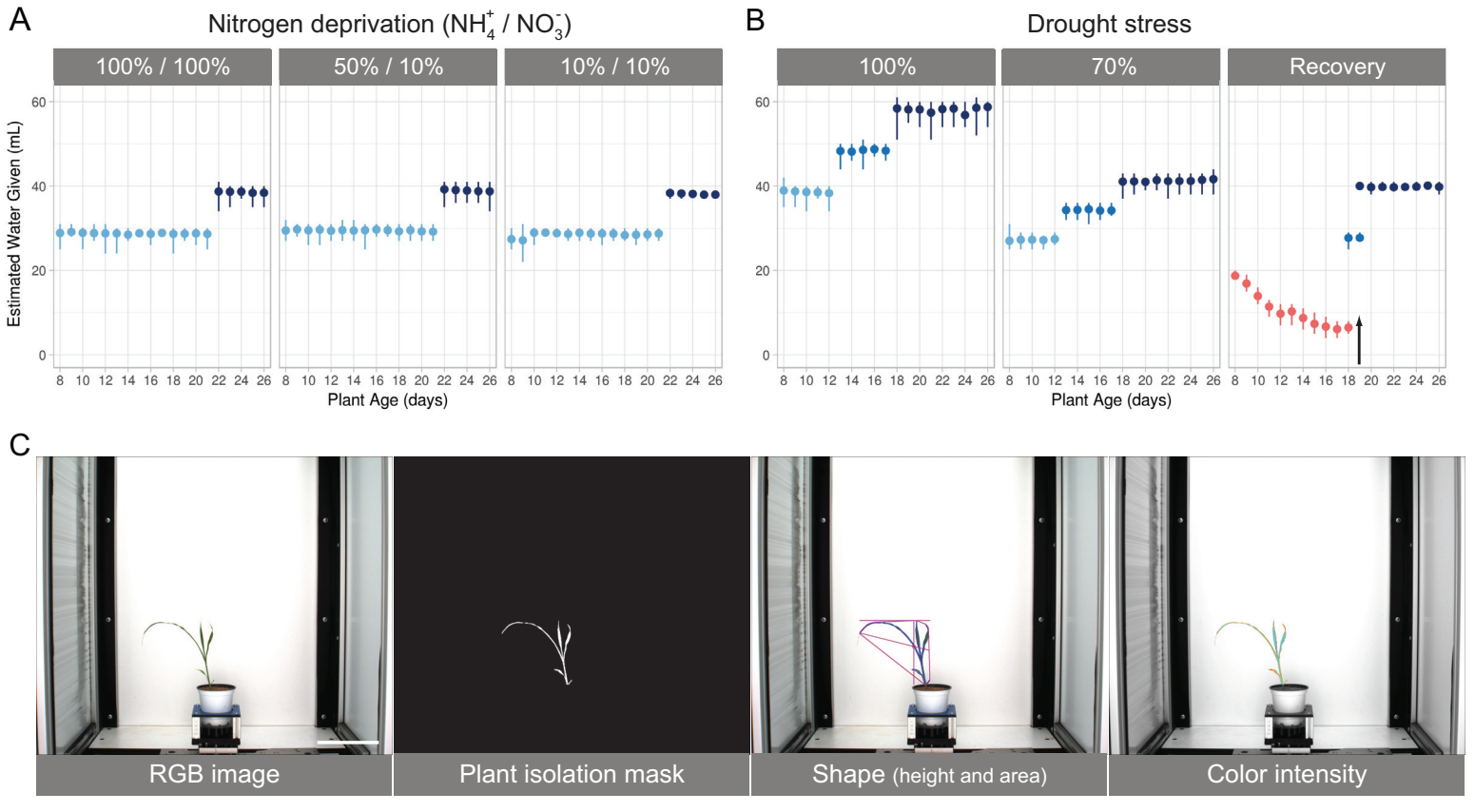
A
Nitrogen deprivation (NH_4^+ / NO_3^-)
100% / 100%
50% / 10%
10% / 10%
Estimated Water Given (mL)
Plant Age (days)
B
Drought stress
100%
70%
Recovery
Plant Age (days)
C
RGB image
Plant isolation mask
Shape (height and area)
Color intensity

A

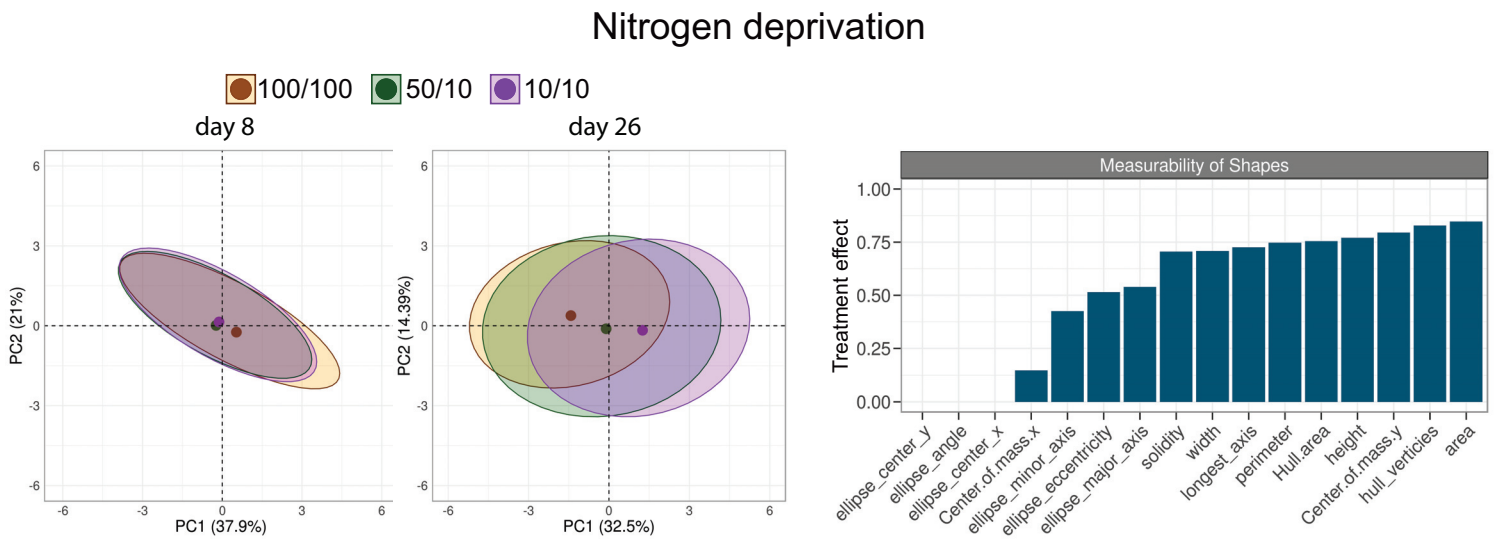

B

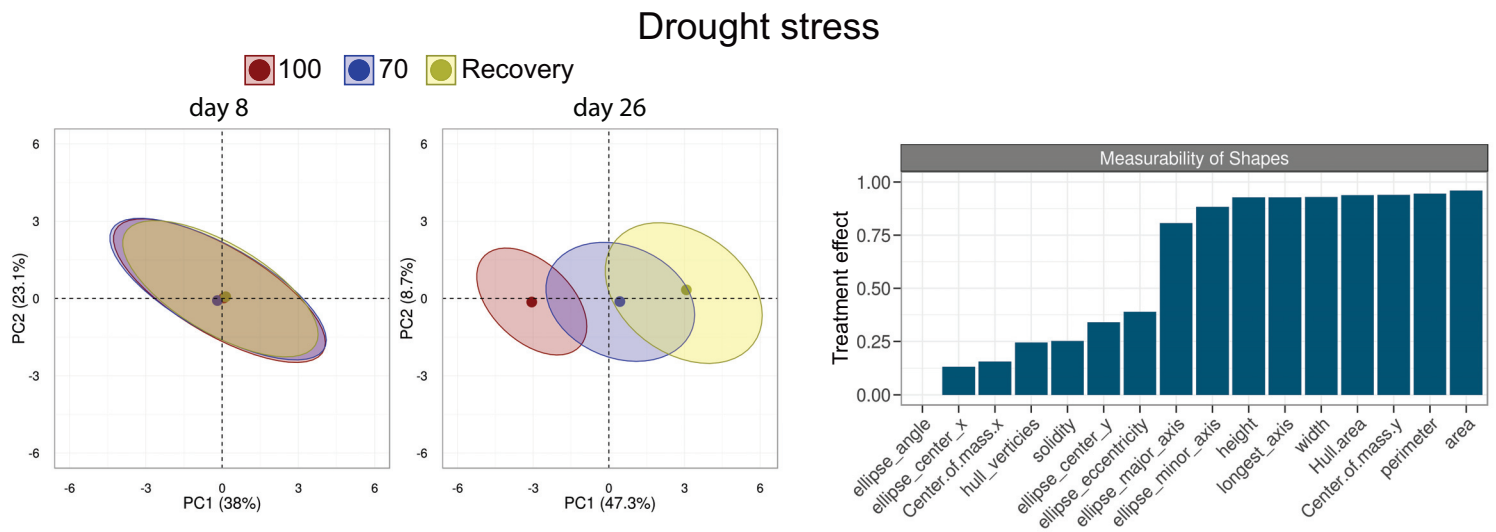

C

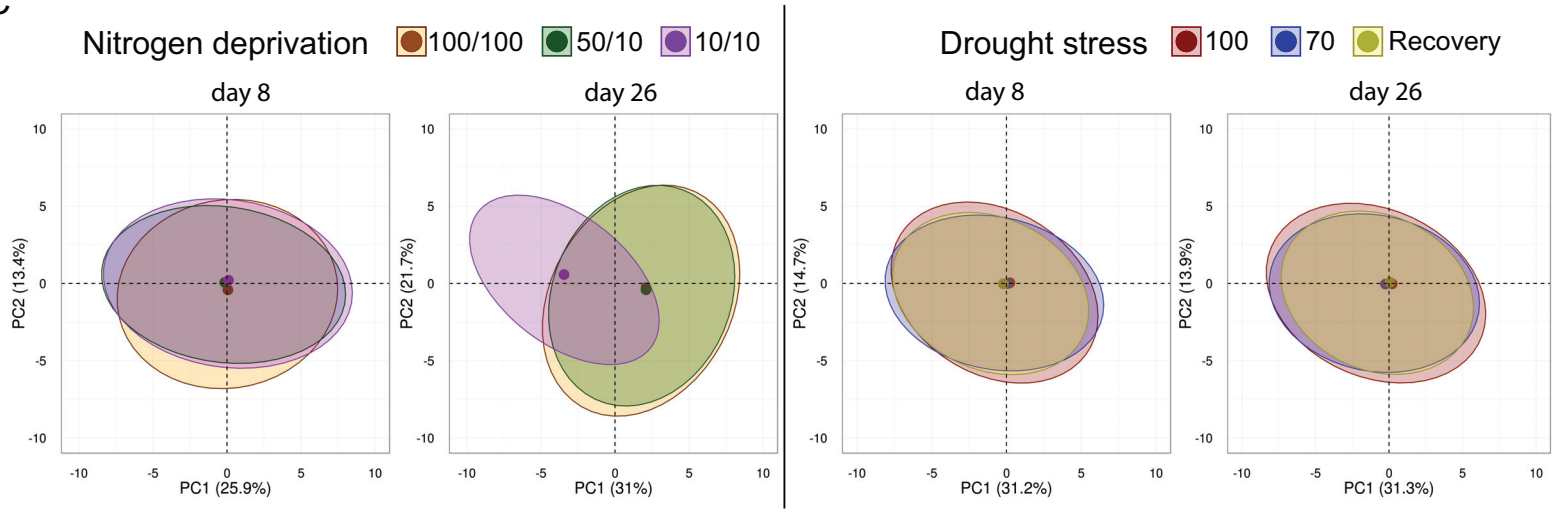

A

Genotype

Source	Chisq	DF	p-value
Nitrogen	415.9	3	<0.0001
Genotype	130.1	29	<0.0001
Nitrogen x Genotype	79.27	58	0.033
Nitrogen x Time	10516	3	<0.0001
Genotype x Time	197.4	29	<0.0001
Nitrogen x Genotype x Time	91.93	58	**0.003**

Type

Source	Chisq	DF	p-value
Nitrogen	1875	3	<0.0001
Type	12.86	2	0.002
Nitrogen x Type	1.844	4	0.764
Nitrogen x Time	4085	3	<0.0001
Type x Time	16.51	2	0.001
Nitrogen x Type x Time	2.321	4	0.677

Photoperiod

Source	Chisq	DF	p-value
Nitrogen	3512	3	<0.0001
Photoperiod	9.017	1	0.003
Nitrogen x Photoperiod	9.147	2	0.01
Nitrogen x Time	7963	3	<0.0001
Photoperiod x Time	1.499	1	0.221
Nitrogen x Photoperiod x Time	7.585	2	**0.023**

Race

Source	Chisq	DF	p-value
Nitrogen	2298	3	<0.0001
Race	26.6	9	0.002
Nitrogen x Race	20.06	18	0.329
Nitrogen x Time	5338	3	<0.0001
Race x Time	39.95	9	<0.0001
Nitrogen x Race x Time	17.55	18	0.486

B

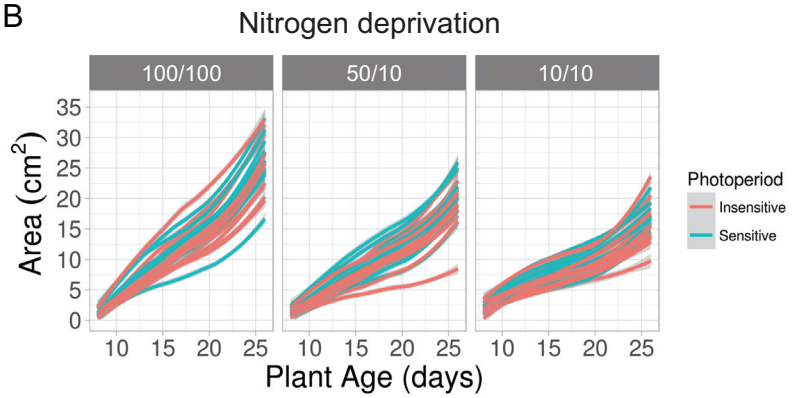

C

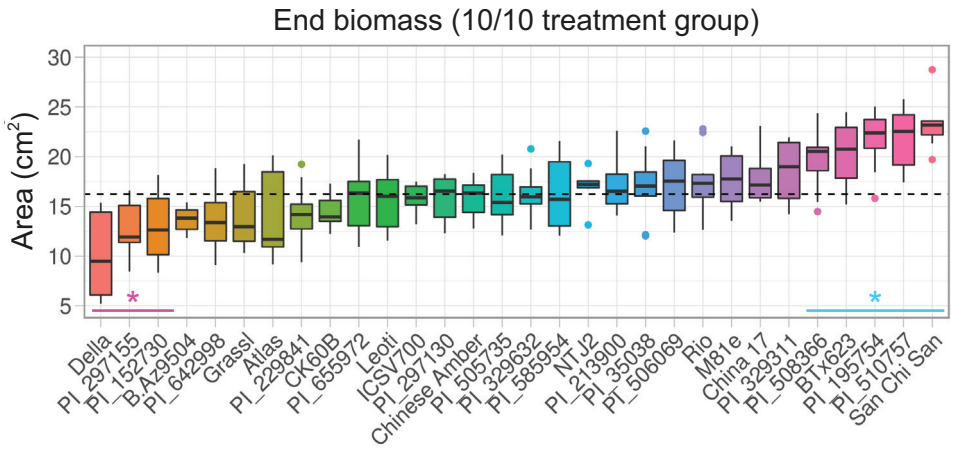

D

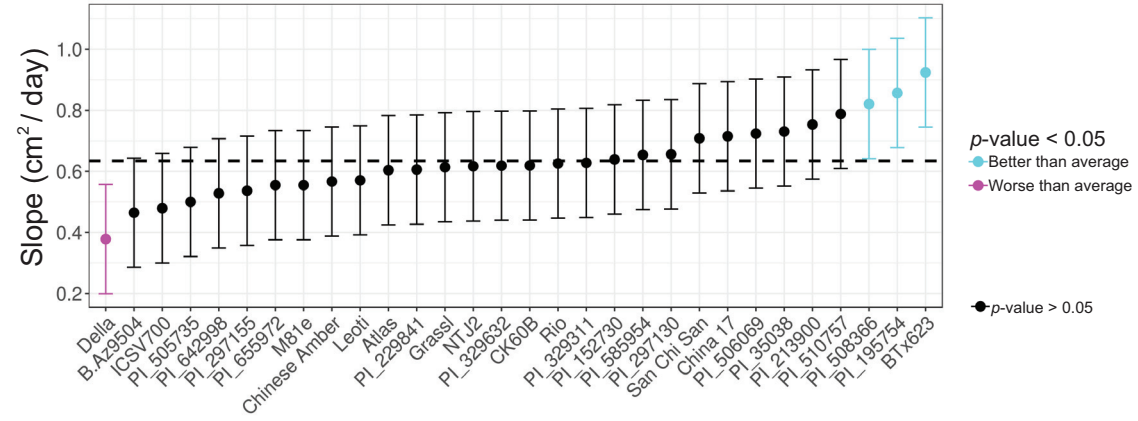

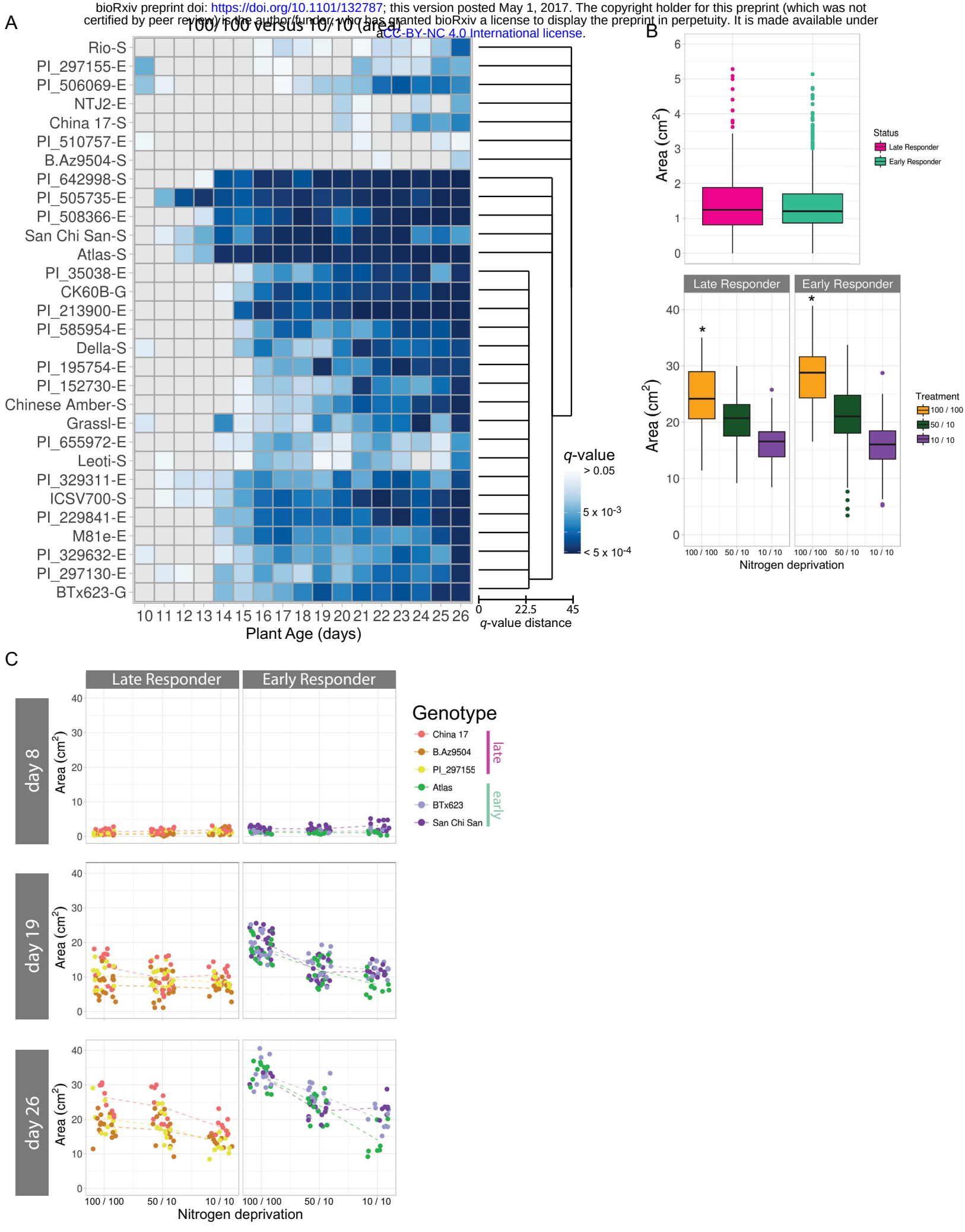

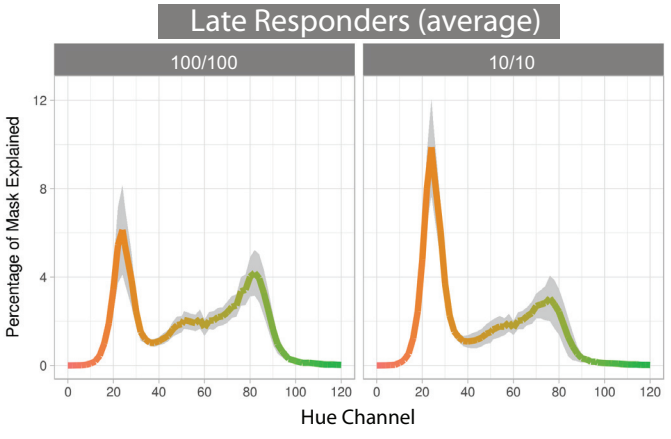
Late Responders (average)
100/100
10/10
Percentage of Mask Explained
Hue Channel

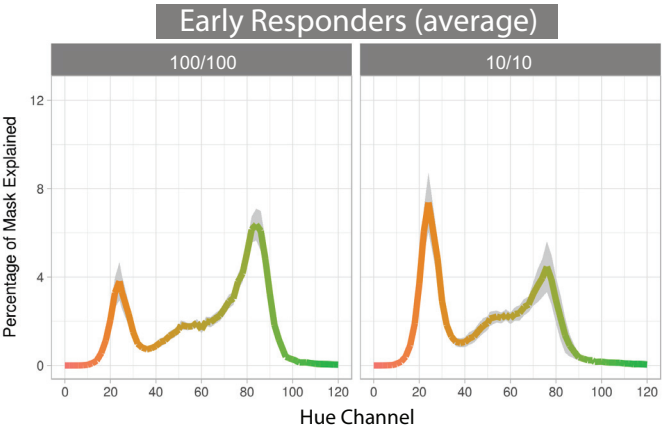
Early Responders (average)
100/100
10/10
Percentage of Mask Explained
Hue Channel

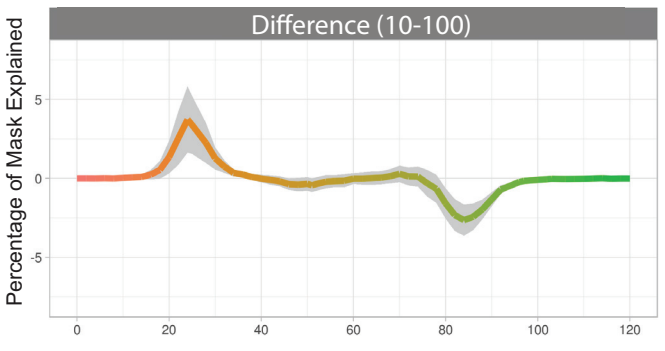
Difference (10-100)
Percentage of Mask Explained

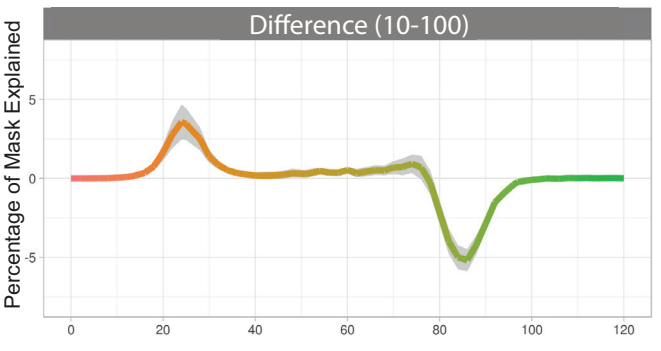
Difference (10-100)
Percentage of Mask Explained

A

Genotype

Source	Chisq	DF	p-value
Water	15042	2	<0.0001
Genotype	229.6	29	<0.0001
Water x Genotype	42.72	29	0.0483
Water x Time	8860	2	<0.0001
Genotype x Time	152.5	29	<0.0001
Water x Genotype x Time	39.51	29	**0.0923**

Type

Source	Chisq	DF	p-value
Water	5004	2	<0.0001
Genotype	6.502	2	0.03874
Water x Type	1.608	2	0.44756
Water x Time	3278	2	<0.0001
Type x Time	5.684	2	0.05831
Water x Type x Time	2.071	2	0.35502

Photoperiod

Source	Chisq	DF	p-value
Water	10918	2	<0.0001
Photoperiod	9.966	1	0.0016
Water x Photoperiod	2.191	1	0.1388
Water x Time	7133	2	<0.0001
Photoperiod x Time	6.879	1	0.0087
Water x Photoperiod x Time	0.165	1	0.6849

Race

Source	Chisq	DF	p-value
Water	7387	2	<0.0001
Race	87.8	9	<0.0001
Water x Race	7.626	9	0.5722
Water x Time	4296	2	<0.0001
Race x Time	56.44	9	<0.0001
Water x Race x Time	9.93	9	0.3562

B

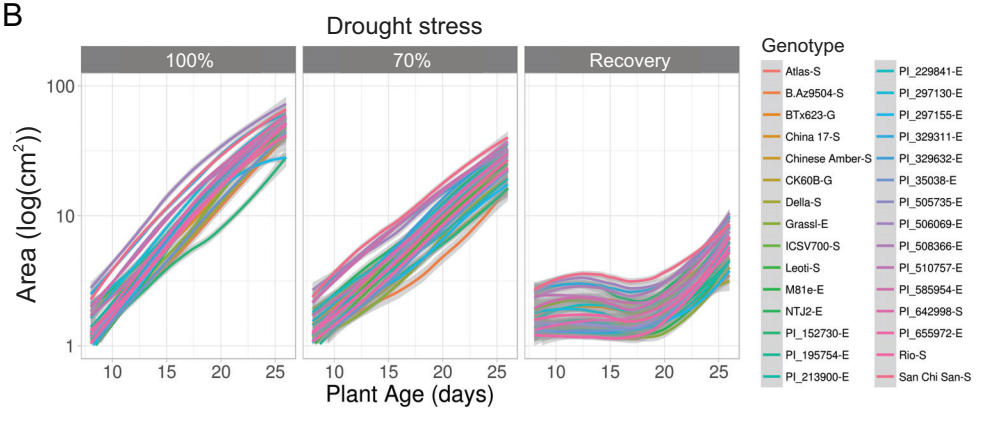

C

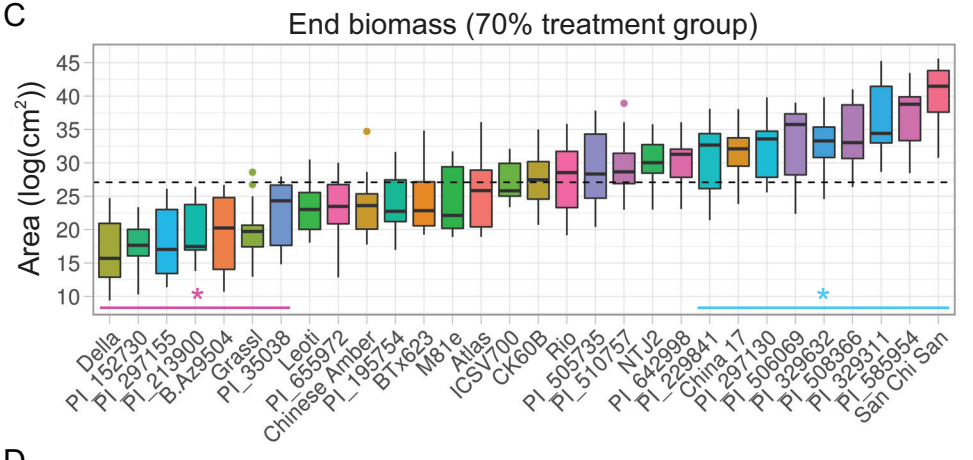

D

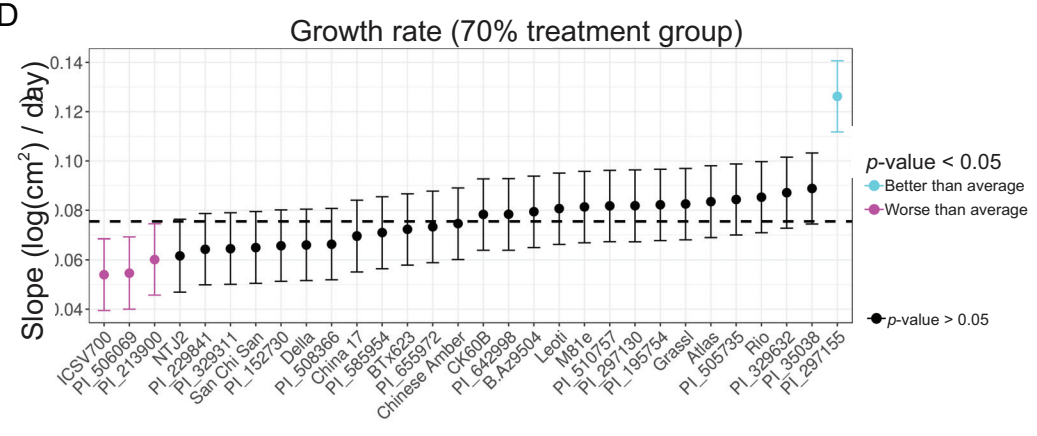

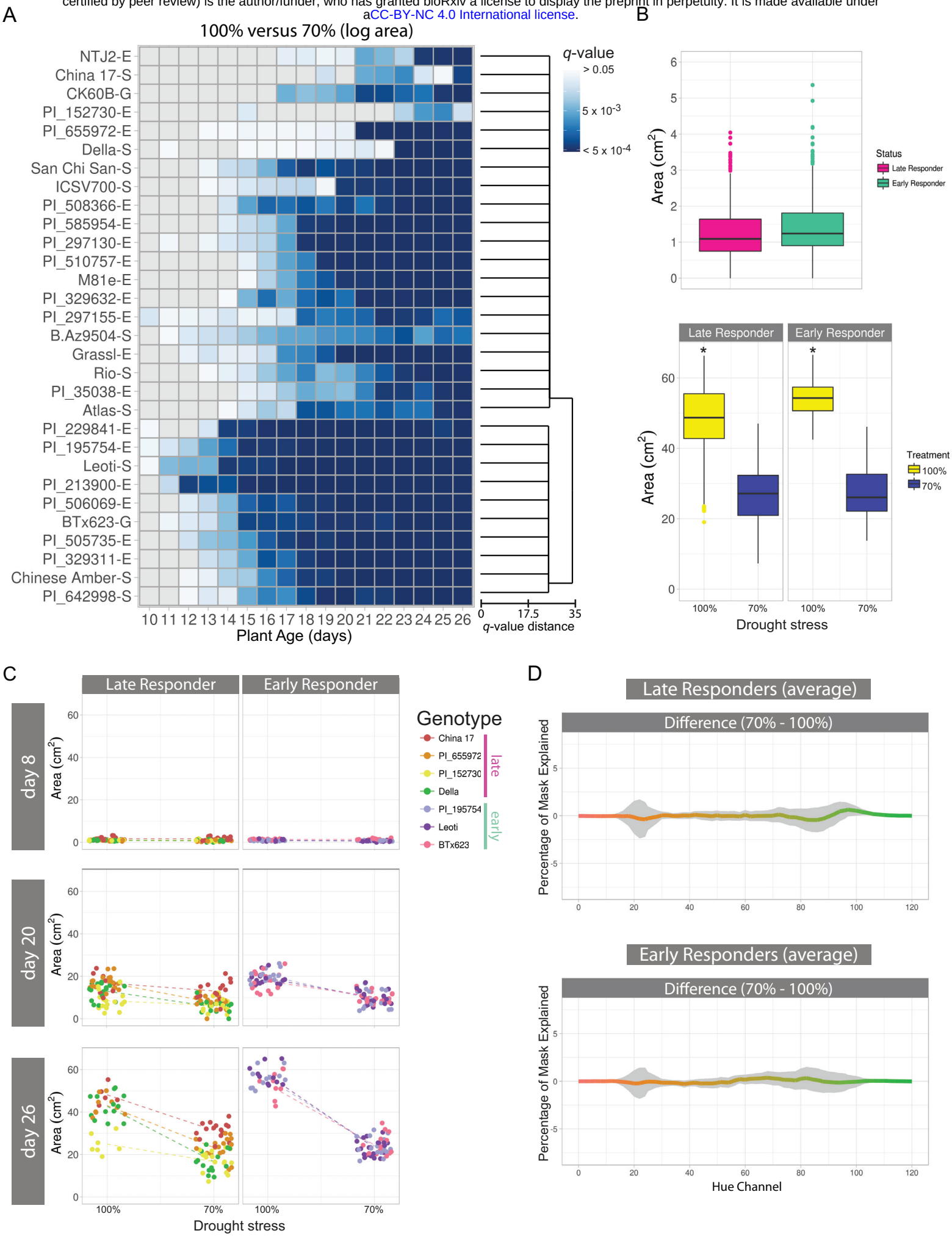

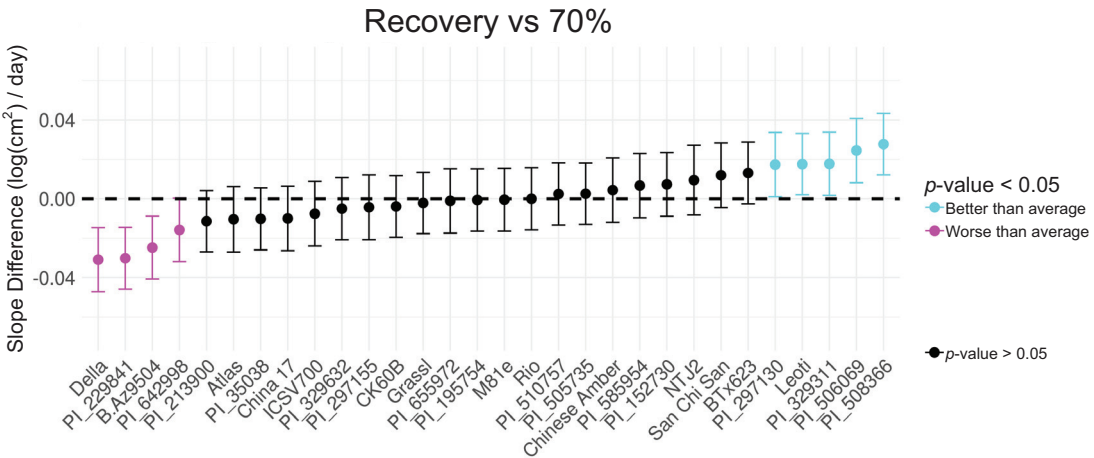
Recovery vs 70%
Slope Difference (log(cm^2) / day)
0.04
0.00
-0.04
Della
PI_229841
B.Az9504
PI_642998
PI_213900
Atlas
PI_35038
China 17
ICSV700
PI_329632
PI_297155
CK60B
Grassl
PI_655972
PI_195754
M81e
Rio
PI_510757
PI_505735
Chinese Amber
PI_585954
PI_152730
NTJ2
San Chi San
BTx623
PI_297130
Leoti
PI_329311
PI_506069
PI_508366
p-value < 0.05
Better than average
Worse than average
p-value > 0.05

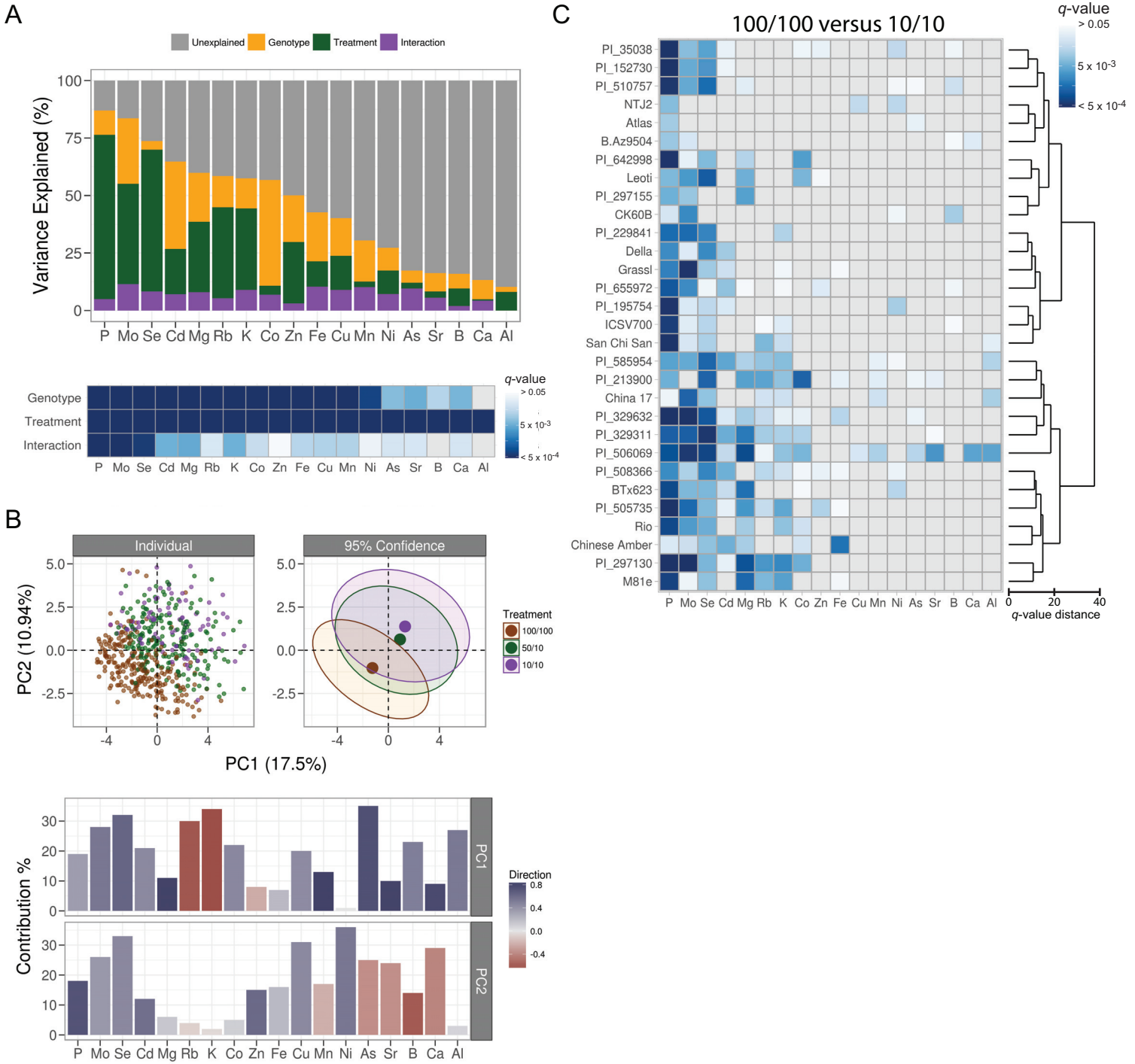
A
Unexplained
Genotype
Treatment
Interaction
Variance Explained (%)
100
75
50
25
0
P Mo Se Cd Mg Rb K Co Zn Fe Cu Mn Ni As Sr B Ca Al
q-value
> 0.05
5 x 10-3
< 5 x 10-4
Genotype
Treatment
Interaction
P Mo Se Cd Mg Rb K Co Zn Fe Cu Mn Ni As Sr B Ca Al
B
Individual
95% Confidence
PC2 (10.94%)
PC1 (17.5%)
5.0
2.5
0.0
-2.5
-4
0
4
Treatment
100/100
50/10
10/10
Contribution %
30
20
10
0
PC1
PC2
Direction
0.8
0.4
0.0
-0.4
P Mo Se Cd Mg Rb K Co Zn Fe Cu Mn Ni As Sr B Ca Al
C
100/100 versus 10/10
q-value
> 0.05
5 x 10-3
< 5 x 10-4
PI_35038
PI_152730
PI_510757
NTJ2
Atlas
B.Az9504
PI_642998
Leoti
PI_297155
CK60B
PI_229841
Della
Grassl
PI_655972
PI_195754
ICSV700
San Chi San
PI_585954
PI_213900
China 17
PI_329632
PI_329311
PI_506069
PI_508366
BTx623
PI_505735
Rio
Chinese Amber
PI_297130
M81e
P Mo Se Cd Mg Rb K Co Zn Fe Cu Mn Ni As Sr B Ca Al
0
20
40
q-value distance

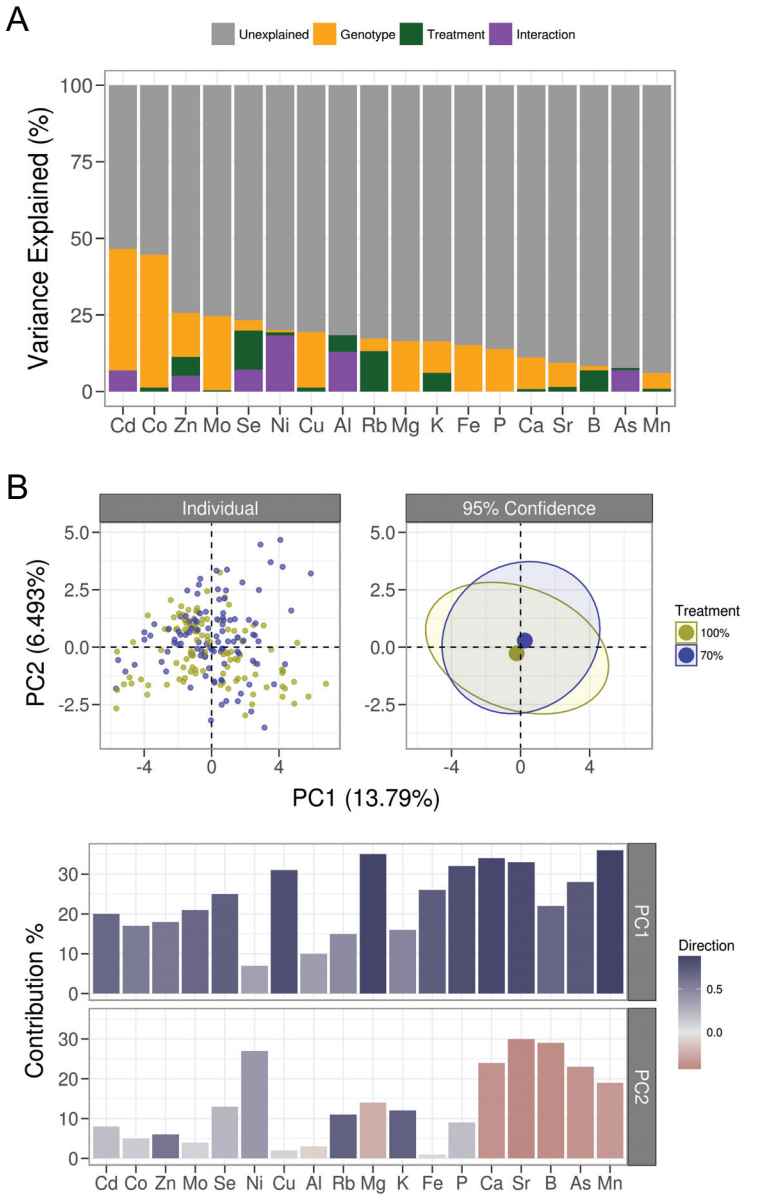
A
Unexplained
Genotype
Treatment
Interaction
Variance Explained (%)
100
75
50
25
0
Cd Co Zn Mo Se Ni Cu Al Rb Mg K Fe P Ca Sr B As Mn
B
Individual
95% Confidence
PC2 (6.493%)
5.0
2.5
0.0
-2.5
-4
0
4
PC1 (13.79%)
Treatment
100%
70%
Contribution %
30
20
10
0
PC1
PC2
Direction
0.5
0.0
Cd Co Zn Mo Se Ni Cu Al Rb Mg K Fe P Ca Sr B As Mn